JOURNAL OF AIRCRAFT
Vol. 38, No. 1, January–February 2001

Low-Speed Natural-Laminar-Flow Airfoils: Case Study in Inverse Airfoil Design

Ashok Gopalarathnam* and Michael S. Selig†
University of Illinois at Urbana–Champaign, Urbana, Illinois 61801

A systematic study of the trends in low-speed natural-laminar-flow airfoils for general aviation applications is presented. The airfoils have been designed using a multipoint inverse airfoil design method, which allows for specification of velocity and boundary-layer properties over different portions of the airfoil. A panel method with a coupled boundary-layer scheme is used to analyze the characteristics of the resulting airfoils. By systematically adjusting the specifications, families of airfoils have been designed with different lift, drag, and pitching-moment characteristics. Parametric studies are presented to study the tradeoffs involved in designing laminar-flow airfoils for general aviation. Although the results of the study are specific to the class of airplanes considered, the design philosophies and the design approach used in the study are applicable to a wide range of airplanes. In addition, the examples presented in the paper form an excellent case study to demonstrate the power of modern inverse design techniques in controlling the performance of an airfoil to a fine degree and in generating a custom database of airfoils suitable for airplane multidisciplinary optimization and trade studies.

Nomenclature

C_d	=	airfoil profile drag coefficient
C_l	=	airfoil lift coefficient
C_l^*	=	design lift coefficient for a segment
C_m	=	airfoil pitching moment coefficient about quarter chord
c	=	airfoil chord
H	=	boundary-layer shape factor
L	=	airplane lift
M	=	Mach number
n	=	laminar boundary-layer transition amplification factor
Re	=	Reynolds number based on airfoil chord
V	=	airfoil velocity nondimensionalized by the freestream velocity
v	=	velocity at a segment endpoint at the design angle of attack of the segment
W	=	airplane weight
x_{tr}	=	chordwise transition location
α	=	angle of attack, deg
α_{0l}	=	zero-lift angle of attack, deg
α^*	=	design angle of attack for a segment, deg

Subscripts

crit	=	denotes critical value for transition
1	=	denotes endpoint of segment 1

Introduction

NATURAL-LAMINAR-FLOW (NLF) airfoils have been in use on high-performance sailplanes for several decades. The popularity of NLF airfoils for general-aviation applications is comparatively more recent following the demonstration[1] of the significant gains in performance that can be obtained by the use of NLF airfoils for wings. Since that time, several airplanes have been designed to use wings with NLF airfoils. Many of these airplanes, however, use airfoils from catalogs[2,3] and other sources.[4] With improvements in rapid, interactive airfoil design methods[4–8] and fast, robust viscous analysis methods,[7] it is now possible to design airfoils tailored to suit an individual application, rather than pick the best-available airfoil from a catalog.

With the increasing popularity of custom-designing NLF airfoils for each application, it is instructive to perform a systematic study of the trends in NLF airfoils for general aviation applications and in doing so illustrate the use of a modern inverse airfoil design method. A study that brings out the tradeoffs involved in designing such airfoils would be useful not only to airfoil designers but also to aircraft designers who can benefit by being better able to lay down the design requirements for a candidate airfoil for their airplane concept. Equally illustrative would be a design approach that can allow designers to rapidly tailor the characteristics of an airfoil to suit a specific application. The present work aims to satisfy both these objectives by using an inverse design approach to perform a systematic parametric study of low-speed NLF airfoils.

It is well known[4,9,10] that the performance of an airfoil can be traced back to the velocity (or pressure) distribution of the airfoil at the design angles of attack. An inverse airfoil method that allows a designer to specify the velocity distribution(s) in some convenient fashion and determine the shape of the airfoil that satisfies the specification(s) is, therefore, of significant value in airfoil design. Quite often, however, a designer wishes to specify not the velocity but the boundary-layer development over some portion of the airfoil at some operating condition. In addition, other constraints such as maximum thickness, leading-edge shape, and pitching moment are almost always part of the design problem.

An example of a modern inverse airfoil design method that can handle specifications on velocity and boundary-layer behavior and simultaneously allow for prescriptions on pitching moment and geometry parameters such as maximum thickness is PROFOIL,[5,6] which has been used to design the airfoils for the systematic study in the current work. The strength of PROFOIL is inverse design (not analysis). To obtain detailed viscous performance of the airfoils designed using PROFOIL, they have been analyzed using XFOIL,[7] which uses a linear-vorticity panel method coupled with an integral boundary-layer solver using a global Newton scheme. The analyses using XFOIL were performed both for the free transition case and with transition fixed at the airfoil leading edge to simulate leading-edge roughness effects, following the recommendation[11] that fixed transition analyses be included as a standard procedure in laminar-airfoil research. Using this approach, it is possible to design an

Received 28 February 1999; revision received 20 July 2000; accepted for publication 17 June 2000.

*Graduate Research Assistant, Department of Aeronautical and Astronautical Engineering; currently Assistant Professor, Department of Mechanical and Aerospace Engineering, North Carolina State University, Box 7910, Raleigh, NC 27695-7910; ashok_g@ncsu.edu. Member AIAA.

†Associate Professor, Department of Aeronautical and Astronautical Engineering, 306 Talbot Laboratory, 104 S. Wright Street; m-selig@uiuc.edu. Senior Member AIAA.

airfoil using PROFOIL in a few seconds and complete the computation for an entire polar using XFOIL in less than 10 min on a personal computer.

The following section discusses the design approach in greater detail. A systematic parametric study of NLF airfoils is then presented using a baseline airfoil suitable for a hypothetical light general aviation airplane with a wing loading of approximately 12–14 lb/ft^2 (576–672 N/m^2). The aim of this study is not to recommend the airfoils for any specific general aviation aircraft, but to illustrate the benefit of posing the airfoil design problem in terms of design variables similar to those used in the current inverse approach. Although the results of the systematic study can be used to understand the tradeoffs involved in NLF airfoil design for the class of airplanes under consideration, it is intended that they serve a greater objective of demonstrating the power of inverse design in rapidly tailoring the characteristics of an airfoil.

Approach

In the current work, the inverse airfoil design method PROFOIL[5,6] has been used to design the airfoils for the parametric study. The XFOIL[7] code has been used as a postdesign analysis tool to obtain the lift, drag, and pitching-moment characteristics of the airfoils over a range of angles of attack. The following subsections describe in detail the relevant features of the two codes.

PROFOIL

PROFOIL is a multipoint inverse design method based on conformal mapping. In the method, the airfoil is divided into several segments. Over each segment, the design angle of attack α^* (pronounced alpha-star) relative to the zero-lift line is prescribed along with the velocity distribution at this design angle of attack. The concept of using several segments for an airfoil, each with its own α^* was first pioneered by Eppler[4] and has been adapted in PROFOIL.[5,6] Because α^* is defined relative to the zero-lift line of the airfoil and the slope of the lift curve is almost exactly equal to 2π per radian, it follows that specifying the α^* is nearly equivalent to specifying the design lift coefficient C_l^* for the segment, that is,

$$C_l^* \approx 0.1 \times \alpha^* \tag{1}$$

where α^* is in deg. The most commonly used (and default) option for the velocity distribution over a segment at its design angle of attack is a constant velocity over the entire segment. In such a case, when the airfoil is operating at a lift coefficient equal to C_l^*, the velocity gradient over the segment is exactly zero. To better understand the implication of such a specification, consider the three airfoils A, B, and C shown in Fig. 1a and focus on the segment on the upper surface extending from 2 to 50% chord (0.02–$0.50c$).

The specifications for the three airfoils are identical except for the values of α^* on the upper-surface forward segment, which are 4, 5, and 6 deg for the airfoils A, B, and C, respectively. Also shown in Fig. 1a are the inviscid velocity distributions for the three airfoils at $\alpha = 5$ deg relative to the zero-lift lines (equivalently, $C_l \approx 0.5$). It can be seen that airfoil B, for which the α^* on the segment is equal to the α under consideration, has zero velocity gradient over the entire segment. When $\alpha > \alpha^*$ for the segment on the upper surface (airfoil A), the velocity gradient is adverse and vice versa (airfoil C). (For segments on the lower surface, changing the lower-surface α^* has the reverse effect on the velocity gradient.)

Consider now the performance of these three airfoils at a Reynolds number of 9×10^6. Figure 1b shows the drag polars, lift, and pitching-moment curves and the upper-surface transition curves for the three airfoils for a C_l range from 0.2 to 0.8. Examination of the upper-surface transition curves in Fig. 1b shows that the zero velocity gradient over the segment under consideration for airfoil B at a C_l of 0.5 has resulted in laminar flow extending to the downstream end of the segment ($0.5c$). For airfoil A, the adverse velocity gradient over the segment at a C_l of 0.5 has resulted in a more upstream location of transition as compared with that for airfoil B. Airfoil C, on the other hand, has favorable velocity gradient on the upper

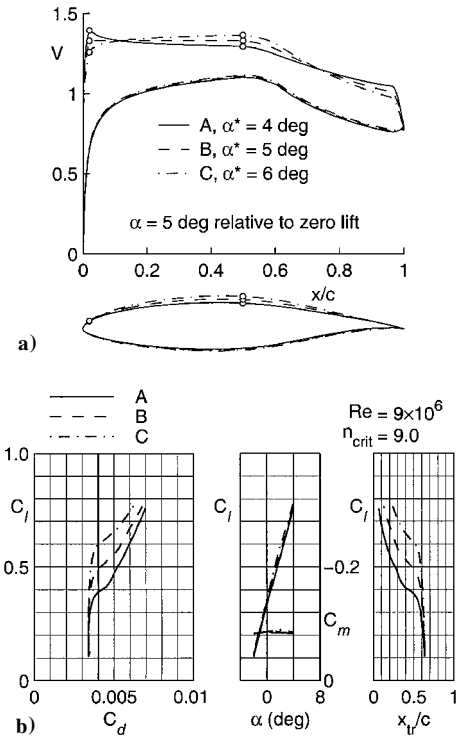

Fig. 1 Illustration of changes in α^*: a) geometries and inviscid velocity distributions for the three example airfoils and b) performance of the three airfoils at $Re = 9 \times 10^6$ predicted using XFOIL.

surface extending beyond $0.5c$ and hence has a transition location downstream of the segment endpoint.

It is also interesting to observe that for all three airfoils the value of the C_l at which laminar flow extends to the downstream end of the segment is almost exactly equal to the corresponding value of the segment C_l^* for that airfoil. In other words, the values of the C_l at which $x_{tr}/c = 0.5$ are close to 0.4, 0.5, and 0.6, which correspond to the segment α^* values of 4, 5, and 6 deg for airfoils A, B, and C, respectively. Thus, by specifying the α^* it is possible to control the velocity gradients, which in turn control the boundary-layer behavior (transition location, in this example) over the segment at its design C_l. The C_d at this C_l therefore can be affected in a logical fashion.

Examination of the geometries of the three airfoils in Fig. 1a shows that increasing the value of α^* for the segment on the upper surface results in an increase in the airfoil thickness. (The reverse is true for segments on the lower surface had the lower-surface α^* values been changed.) Thus varying α^* results in logical variations not only to the velocities but also to the shape.

The examples used in this section were generated solely for illustrating the concept of α^*. For an airfoil for a practical application, it would often be preferable to use several smaller segments with progressively increasing values of α^* toward the leading edge of the airfoil. Using a single large segment on the upper surface could result in a large, abrupt movement of the transition location with increasing C_l, which is usually undesirable.

Because the design angles of attack for an airfoil differ from one segment to another, it is possible to design different portions of the airfoil for different operating conditions. For example, the α^* for segments on the leading-edge portion of the upper surface can be used to tailor the performance at high lift coefficients, while simultaneously the α^* values for the lower surface can be set to adjust the drag behavior at low values of C_l. Thus multipoint inverse design is possible.

An important feature of the method is the multidimensional Newton iteration scheme. The scheme allows the designer to selectively give up control on some of the parameters used in the conformal mapping in order to achieve specified values for other design specifications. As a simple example to control the geometry, it is possible to vary the values of the α^* for all segments on the

upper surface to achieve a desired maximum thickness, while simultaneously varying the α^* values on the lower surface to achieve a desired value of the maximum camber.

In addition to the default constant velocity specification for a segment, PROFOIL allows selection of a nonconstant velocity distribution for any segment at its design angle of attack. In particular, the method allows the prescription of a nonlinear velocity variation over a segment by defining a fixed number of nodes through which a spline is passed.[5,6] By using the multidimensional Newton scheme and an integral boundary-layer method, it is possible to iterate on the velocity values at the nodes of the segment to achieve a desired variation of a boundary-layer parameter, such as the transition amplification factor n for a laminar boundary layer or, say, the shape factor H.

Taken together, the multipoint specification of velocity gradients via α^* values on the different segments, the ability to selectively prescribe boundary-layer properties and the multidimensional Newton iteration scheme make this method a valuable airfoil design tool and well suited to performing parametric studies. In addition, a MATLAB®-based graphical user interface has been developed, which makes it easier to use PROFOIL by allowing the user to interactively edit the α^* distributions using the mouse, run PROFOIL and view the results graphically. Although PROFOIL has excellent inverse design capabilities, its analysis capabilities are limited. An analysis code such as the Eppler code[4] or XFOIL is necessary for detailed postdesign viscous analysis. The following subsection briefly describes the analysis method in XFOIL.

XFOIL

XFOIL[7] is an analysis and design method for subcritical airfoils. In the present work XFOIL version 6.8 has been used as a postdesign viscous/inviscid analysis code. A linear-vorticity panel method is used for inviscid analysis in XFOIL. This panel method is coupled with an integral boundary-layer method and an e^n-type transition amplification formulation using a global Newton method to compute the viscous performance of the airfoil. XFOIL has proven to be well suited to rapid analysis of subcritical airfoils even in the presence of significant transitional separation bubbles.[7]

In the present work all airfoils have been analyzed with 200 panels distributed using XFOIL's paneling routine. In addition, where necessary, panels have been bunched around the transition locations to provide adequate resolution of any separation bubbles. To obtain an estimate of the reliability of XFOIL in predicting the characteristics of NLF airfoils, predicted results for two airfoils have been compared with experimental results from wind-tunnel tests. Figure 2a shows a comparison of the predicted lift, drag, pitching-moment, and upper- and lower-surface transition characteristics for the 16%-thick NASA NLF(1)-0416 airfoil with wind-tunnel results[12] from the NASA Low-Turbulence Pressure Tunnel (LTPT) at a Reynolds number of 1×10^6. Figure 2b shows a comparison of the characteristics for the 15%-thick NLF(1)-0215F airfoil with experimental results[13] from the NASA LTPT at a Reynolds number of 3×10^6. Experimental transition curves were not available for the NLF(1)-0215F airfoil. The geometries for the two airfoils are shown in Fig. 2c. The figures show that compared with the experimental results, the C_l values at angles of attack close to stall are overpredicted by XFOIL by about 0.1 at $C_{l,\max}$. The C_d values for the low-drag range, C_l values for the corners of the low-drag range, and the lift, pitching-moment, and transition curves from XFOIL computations agree quite well with the experimental results. Based on these comparisons and past experience, it is believed that XFOIL is well suited to making comparison of the trends in performance characteristics of airfoils with systematically varying design specifications.

Baseline Airfoil Characteristics

A common airfoil has been used as a baseline in all parts of the parametric study in this paper. This baseline airfoil has been designed to suit a hypothetical light general aviation airplane with a wing loading in the range 12–14 lb/ft^2 (576–672 N/m^2). This section describes the design goals, implementation, and the predicted performance characteristics for the baseline airfoil. All XFOIL performance plots in this section and the rest of the paper are presented at constant values of $Re\sqrt{C_l}$ and $M\sqrt{C_l}$. Using these "reduced" Reynolds and Mach numbers ensures that the variations of Reynolds and Mach numbers with C_l closely mimic those experienced by the airfoil in flight. These relationships for reduced Reynolds and Mach numbers can be derived from $L \approx W$ considerations for an airplane in steady rectilinear flight.

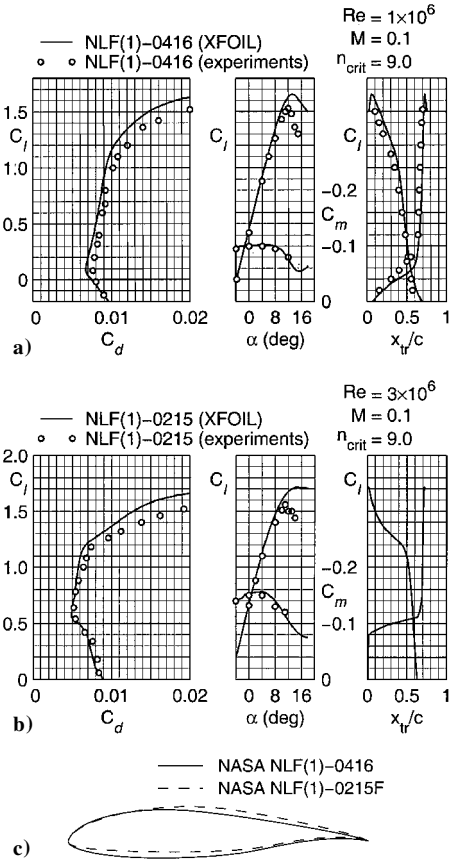

Fig. 2 Comparison of predicted and experimental characteristics for two airfoils: a) for the NASA NLF(1)-0416 airfoil, b) for the NASA NLF(1)-0215F airfoil, and c) airfoil shapes.

The design goals for the baseline airfoil are listed next: 1) design $Re\sqrt{C_l}$ of 2 million, 2) design $M\sqrt{C_l}$ of 0.1, 3) airfoil maximum thickness of 14%, 4) laminar flow to at least $0.5c$ on both surfaces within the low-drag range (drag bucket), 5) lower corner of the low-drag range at a C_l of 0.25, 6) C_m in the low-drag range not less than -0.090, 7) $C_{l,\max}$ of at least 1.5, and 8) minimize sensitivity of $C_{l,\max}$ to leading-edge roughness.

Figure 3a shows the geometry and the inviscid velocity distributions for the baseline airfoil designed using PROFOIL to meet the design goals. As seen from the figure, the airfoil has been divided into several segments. Some of the important segment endpoints have been labeled in the figure to aid further discussion. Segment endpoints 2 and 17 are the downstream locations of the laminar regions on the upper and lower surfaces of this airfoil, and they correspond to the $0.5c$ location. The segments 2 and 18 are transition ramps, where nonlinear velocity specifications have been used to gradually change the velocity gradient from favorable gradients upstream in the laminar portions to adverse gradients downstream in the recovery portions. These ramps[9,10] are used to avoid or reduce the intensity of transitional separation bubbles that occur in the presence of an abrupt increase in adverse pressure gradient in a laminar boundary layer. As seen from Fig. 3a, the laminar portion on the upper surface has been divided into several segments. The α^* values for these segments increase (gradually at first, then more steeply) from the downstream end of the laminar region to the leading-edge segment 13. Such an α^* variation results in a gradual movement of the upper-surface transition location from $0.5c$ at the

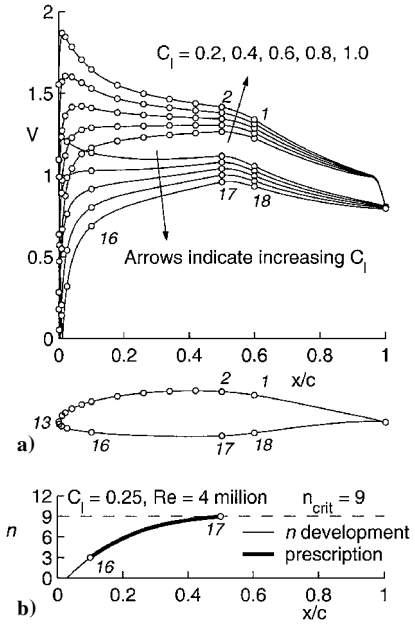

Fig. 3 Characteristics of the baseline airfoil: a) geometry and inviscid velocity distributions for the baseline airfoil (with important segment endpoints labeled) and b) *n* development on the lower surface as computed by PROFOIL compared with the prescription.

C_l corresponding to the upper corner of the low-drag range to the leading edge at $C_{l,\max}$.

By ensuring that the upper-surface transition point occurs naturally at the leading edge at stall, the $C_{l,\max}$ value is made independent of the achievement of a significant amount of laminar flow and is thus relatively independent of leading-edge roughness that might be caused by insect debris.[13–15]

Although it is desirable for the upper-surface transition location to move forward gradually with increasing C_l, there is usually no such requirement for the movement of the lower-surface transition location when the C_l is reduced below that of the lower corner of the drag bucket. For this reason all of the segments on the lower surface are specified to have the same value of α^*. This value has been set at 2.5 deg for the baseline airfoil to anchor the lower corner of the polar at a C_l of 0.25. In addition, the transition amplification factor n at a C_l of 0.25 and Reynolds number of 4×10^6 (corresponding to a C_l of 0.25 and $Re\sqrt{C_l}$ of 2 million) has been prescribed to grow in a nonlinear fashion from a value of 3 at the endpoint of segment 16 to the critical value of 9 by the endpoint of segment 17 as shown in Fig. 3b. Such a prescription for n ensures that while the lower surface has laminar flow to $0.5c$ at a C_l of 0.25 the laminar boundary layer upstream of this point is close to transition. The computation of the n growth in the PROFOIL code[5,6] for a given velocity distribution is similar to the method used in XFOIL.[7] This method uses an empirical relation from Ref. 16, which is a correlation of spatial growth rates computed from solutions to the Orr–Sommerfeld equation. Having set the lower-surface α^* values at 2.5 deg, the Newton iteration scheme is used to adjust the α^* values for the segments on the upper surface to achieve the desired thickness of 14%. In addition, the velocity level of the first segment v_1, which indirectly determines the aft loading on the airfoil, is adjusted[5,6] to achieve a zero-lift C_m of -0.09.

The performance of the baseline airfoil as predicted by XFOIL is shown in Fig. 4 for both the clean case (free transition) and with simulated leading-edge roughness, where transition has been fixed at $0.05c$ on the upper surface and $0.1c$ on the lower surface. Examination of these results shows that the design goals for the baseline airfoil have been successfully met. Comparing the performance of the airfoil with and without simulated leading-edge roughness shows that although the drag increases in the rough condition resulting from a loss in the laminar flow there is no loss in the $C_{l,\max}$ because the upper surface has fully turbulent flow at this C_l even when clean.

Table 1 Design prescriptions for the lower- and higher-lift versions compared with the baseline values

Airfoil	Lower-surface α^*, deg	Lower-surface design Re	α_{0l}, deg
Lower lift	1.5	5.1×10^6	−2.7
Baseline	2.5	4×10^6	−3.7
Higher lift	3.5	3.4×10^6	−4.7

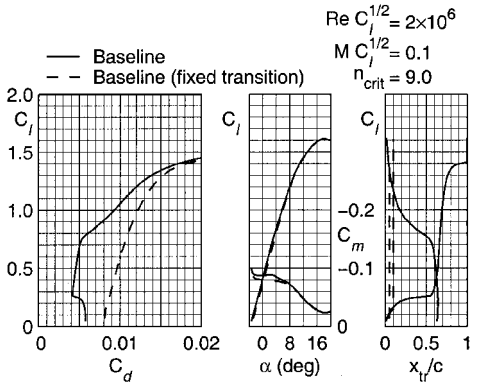

Fig. 4 Performance of the baseline airfoil with free and fixed leading-edge transition predicted using XFOIL.

Parametric Study

This section discusses the systematic four-part parametric study. The four design variables are listed first. These four variables have been chosen as examples to illustrate the logical effect that the baseline-airfoil design variables have in systematically altering the airfoil performance. The effect of adjusting each of the design variables from their baseline values is then examined in detail by comparing the geometries, inviscid velocity distributions, and the predicted characteristics from XFOIL analyses of the resulting airfoils with those of the baseline. The XFOIL computations for all of the airfoils in this parametric study have been conducted at a $Re\sqrt{C_l}$ of 2 million, $M\sqrt{C_l}$ of 0.1, and n_{crit} of 9. Where relevant, the predicted performance comparisons have also been presented with simulated leading-edge roughness by analyzing the airfoils using XFOIL with transition fixed at $0.05c$ on the upper surface and $0.1c$ on the lower surface.

Design Variables

The design variables used in the parametric study are 1) the α^* value used for the lower-surface, 2) the maximum thickness prescription, 3) the pitching-moment prescription, and 4) the extent of laminar flow on the upper and lower surfaces.

Effect of Changing the Lower-Surface α^*

As mentioned in the preceding section, the lower-surface α^* value for the baseline airfoil was fixed at 2.5 deg to anchor the lower corner of the polar at a C_l of 0.25. In this part of the parametric study, this value of the lower-surface α^* has been varied by ± 1 deg to design lower- and higher-lift versions of the baseline airfoil. Because the design of the lower surface is determined not only by the lower-surface α^* values but also by the n-development prescription shown in Fig. 3b, the Reynolds number for this prescription has to be altered from the baseline value of 4×10^6 to be consistent with the use of a $Re\sqrt{C_l}$ of 2 million. In addition to these variations, the aft loading on the two airfoils has been adjusted from the baseline case. This adjustment is desired to maintain similar velocity gradients in the recovery regions for all three airfoils. To adjust the aft loading in a systematic fashion, the values of the zero-lift angle of attack, α_{0l} were prescribed to be 1 deg more and 1 deg less than the baseline value for the lower- and higher-lift versions, respectively. To achieve these α_{0l} prescriptions, the velocity level of the first segment v_1 was selected as the variable in the Newton iteration scheme.[5,6] Table 1

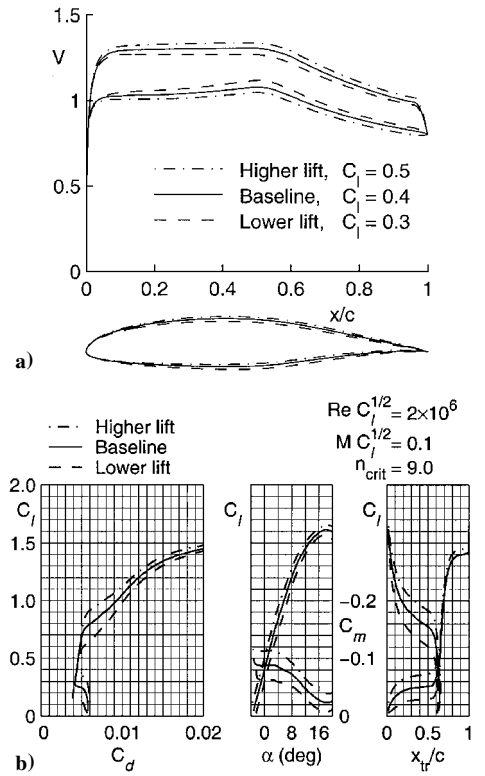

Fig. 5 Effect of changing the lower-surface α^*: a) geometries and inviscid velocity distributions and b) predicted performance in the clean condition.

compares the prescriptions for the two new airfoils with the baseline values.

Figure 5a shows the geometry and the inviscid velocity distributions for the three airfoils. At a glance it might appear that the higher- and lower-lift airfoils could be produced by simple changes in camber. But upon close inspection of the airfoil geometries in Fig. 5a, it can be seen that the airfoils do not differ uniformly by camber alone. It must be kept in mind that these geometry changes were arrived at as a consequence of changes to the baseline aerodynamic prescriptions listed in Table 1 and were not known a priori. The velocity distributions in Fig. 5a for the lower- and higher-lift versions have been plotted for C_l values, which are 0.1 lower and 0.1 higher than the C_l value of 0.4 used for the baseline case. Although the C_l values are different, it is seen that the upper-surface velocity gradients for the three airfoils are similar. Likewise, the lower-surface velocity gradients for the three airfoils resemble each other. It must be remarked that the resemblance is even more striking if the lower-surface design Reynolds-number values were kept the same as opposed to the different values (see Table 1) used in this study. The similarity in the velocity gradients between the airfoils indicates that the performance is also likely to be similar, but at different C_l values. In other words, the lower-lift airfoil at a C_l of 0.3 is likely to have similar aerodynamic performance to that of the baseline airfoil at a C_l of 0.4.

The predicted performance comparison in Fig. 5b shows that the lower corners of the polars for the lower- and higher-lift versions have moved to C_l values of 0.15 and 0.35, respectively, as compared with the baseline value of 0.25. These values correspond to the lift coefficients at which transition rapidly moves forward on the lower surface and are consistent with the lower-surface α^* values of 1.5, 2.5, and 3.5 deg for the three airfoils. Because all three airfoils have the same maximum thickness prescription, the α^* values for segments on the upper surface are automatically varied by the Newton iteration scheme and are shifted by almost exactly -1 deg for the lower-lift case and $+1$ deg for the higher-lift case from their corresponding values for the baseline airfoil. As a consequence, the upper ends of the low-drag range for the three airfoils have also been affected in a logical fashion resulting in nearly equal widths for the low-drag range for the three airfoils.

The performance characteristics of the three airfoils were also compared with simulated leading-edge roughness. The results (not shown) reveal that although the variations in $C_{l,\max}$ between the airfoils are identical to the variations for the clean case; all three airfoils have the same drag polars in the rough condition. This result is a consequence of the drag being determined almost entirely by the transition locations, which are fixed close to the leading edges to simulate roughness effects.

Thus, it is seen that changing the lower-surface design angles of attack results in a shifting of the aerodynamic characteristics by the equivalent C_l. In particular, this design variable can be used to anchor the lower corner of the polar at the design C_l corresponding to the maximum speed of the airplane.

Effect of Changing the Maximum Thickness

The specification of 14% maximum thickness for the baseline airfoil is varied in this section to design a thinner version with 13% and a thicker airfoil with 15% thickness. As mentioned earlier, the α^* values for the upper-surface segments are adjusted automatically by the Newton iteration scheme to achieve these thickness prescriptions. Both the thinner and the thicker versions in this part of the study have the same pitching-moment prescription as the baseline airfoil. Figure 6a shows the geometry and the inviscid velocity distributions

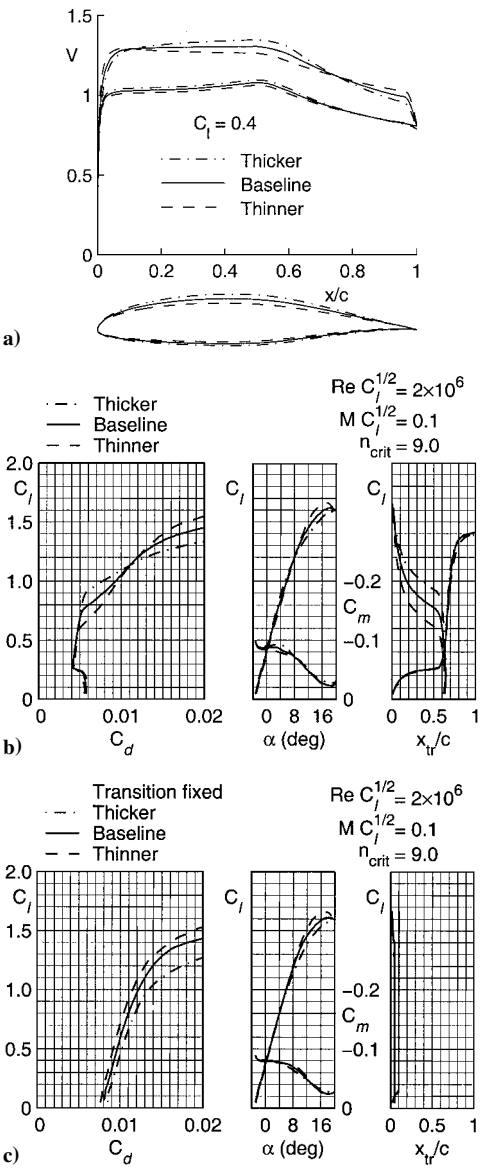

Fig. 6 Effect of changing the maximum thickness: a) geometries and inviscid velocity distributions and predicted performance, b) in the clean condition, and c) with simulated leading-edge roughness.

at a C_l of 0.4. Examination of the velocity distributions shows that although the lower-surface velocities are similar between the three airfoils the velocity gradient on the laminar portion of the upper surface becomes more favorable with increasing thickness. This behavior is a consequence of an increase in the α^* values for the segments on the upper surface with increasing airfoil thickness. The velocity gradients in the upper-surface recovery region, however, become more adverse with increasing thickness to maintain the same pitching moment.

The predicted performance for the three airfoils is compared in Fig. 6b. All of the features of the performance characteristics can be explained with reference to the velocity distributions in Fig. 6a. The lower corners of all the drag polars are fixed at a C_l of 0.25 corresponding to the lower-surface α^* value of 2.5 deg. The pitching moment values in low-drag range for the three airfoils are all close to the prescribed value of -0.09. Because the extents of laminar flow on the upper and lower surfaces are equal for all three airfoils, the C_d values in the low-drag range are also similar and follow the same trend. The thicker airfoils, however, have a larger low-drag range (higher C_l value for the upper corner of the drag bucket) owing to the more favorable velocity gradients in the laminar region of the upper surface. As seen from the figure, this benefit is traded off by the higher C_d at values of C_l close to stall and also a lower $C_{l,\max}$ as a result of the more adverse velocity gradients in the upper-surface recovery regions. The increase in adverse velocity gradients in the upper-surface recovery regions results in an earlier onset of turbulent boundary-layer separation at the trailing edge.

Examination of the polars with simulated leading-edge roughness in Fig. 6c shows that the C_d in the rough condition increases with increasing thickness. This behavior is also a result of the increase in the velocity gradient over the upper-surface recovery region with increasing thickness.

Effect of Changing the Pitching Moment

In this part of the parametric study, the pitching moment of the baseline airfoil has been changed ± 0.03 from the baseline value of -0.090. As mentioned earlier, the velocity level of the first segment v_1, which determines the aft loading on the airfoil, was selected as the variable in the Newton iteration scheme to achieve these prescriptions on the pitching moment. To avoid abrupt changes in the velocity distributions as a result of the changes in the aft loading, the velocity drops in the transition ramps have been increased on the upper surface and decreased on the lower surface for the lower pitching-moment case (i.e., $C_m = -0.060$ case) and vice versa for the higher pitching-moment airfoil.

Figure 7a shows the geometry and inviscid velocity distributions at a C_l of 0.4, and Fig. 7b shows the performance plots for the three airfoils. It is seen that with increasing C_m (more negative) the velocity distribution becomes less adverse in the upper-surface recovery region and more adverse in the lower-surface recovery region. The consequence, as seen from the performance plot, is an increase in the $C_{l,\max}$ with increasing pitching moment. This benefit has to be traded off against a possible increase in trim drag. The performance was compared for the three airfoils with simulated leading-edge roughness. The results (not shown) indicate that the $C_{l,\max}$ values are identical to the corresponding values for the clean case. All three airfoils with simulated leading-edge roughness have nearly the same C_d over much of the lift range.

Effect of Changing the Laminar Extents

Two airfoils have been designed in this part of the parametric study by increasing both the upper-surface and lower-surface laminar-flow extents by $0.1c$ and decreasing them by the same amounts. The aft loading on the airfoil in this part of the study was specified by prescribing that all three airfoils should have the same velocity value at the end of the recovery region on the upper surface (denoted by point A in Fig. 8a). In addition, the velocity drop in the lower-surface transition ramp has been increased with increasing amounts of laminar flow to avoid abrupt changes in the velocity distribution. The geometry and velocity distributions for a C_l of 0.4 are shown in Fig. 8a. Increasing the laminar extents results

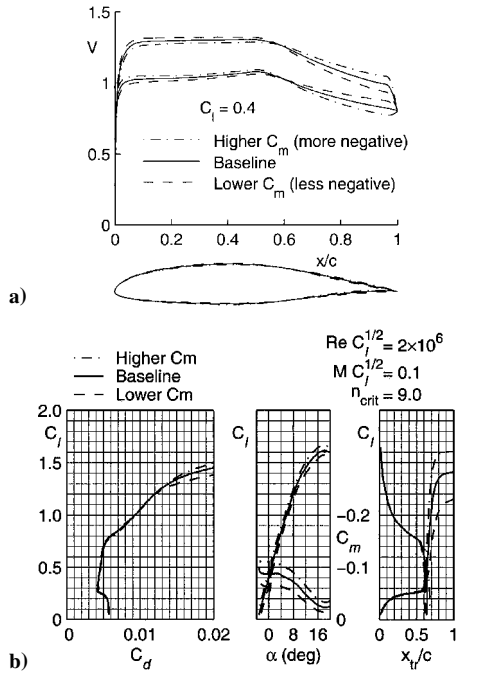

Fig. 7 Effect of changing the pitching moment: a) geometries and inviscid velocity distributions and b) predicted performance in the clean condition.

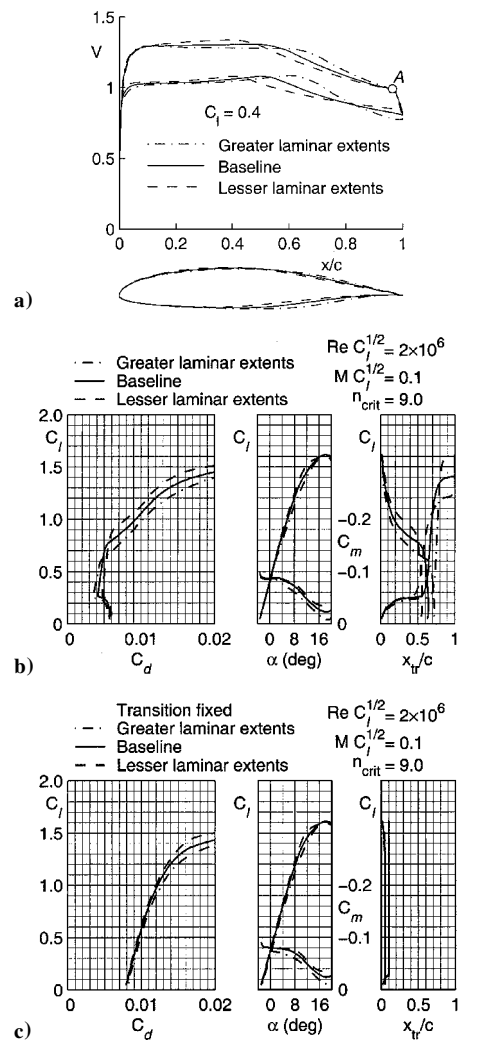

Fig. 8 Effect of changing the laminar extents: a) geometries and inviscid velocity distributions and predicted performance, b) in the clean condition, and c) with simulated leading-edge roughness.

in a shorter distance over which the velocity has to be recovered and hence results in steeper velocity gradients in the recovery regions. In addition, the velocity gradient in the upper-surface laminar region becomes more favorable when the extent of laminar flow is decreased.

The performance plots in Fig. 8b show that although increasing laminar flow results in a reduction in the C_d over the low-drag range this benefit has to be traded off against a decrease in the size of the low-drag range (or the width of the drag bucket). A similar result has also been presented for symmetric airfoils by Wortmann.[10] In addition to lower widths of the low-drag range, increasing the extents of laminar flow (within the range of the laminar-flow extents considered here) also results in an increase in the C_d at high-C_l values and a slight increase in the C_d over the baseline case when leading-edge roughness is simulated (see Fig. 8c).

Conclusions

A multipoint inverse method has been used to perform a systematic study of the trends in low-speed natural-laminar-flow airfoil design. A baseline airfoil was first designed by posing the design problem in terms of velocity and boundary-layer prescriptions over different regions of the airfoil at their design angles of attack, along with specifications on the airfoil maximum thickness and the pitching-moment coefficient. It is shown that these specifications can be systematically altered to generate families of airfoils with logically varying trends. The paper presents a four-part parametric study to show the effects of varying four design variables: the lower corner of the low-drag range, the maximum thickness, the pitching-moment coefficient, and the extents of laminar flow. In each case the inviscid velocity distributions, airfoil shapes, and performance characteristics are presented for both the free-transition case and with simulated leading-edge roughness. These results are then used to study the tradeoffs involved in altering the design variables. The effects of the velocity distributions on the performance are also discussed in detail to provide insight into designing airfoils using an inverse airfoil design method, where the velocity distributions are prescribed rather than the geometry.

It must also be emphasized that the design variables used in the paper can be combined judiciously to tailor an airfoil to suit a particular requirement. For example, it was shown that increasing the thickness results in a loss in $C_{l,\max}$, but this loss in $C_{l,\max}$ can be recovered if an increase in the pitching moment can be tolerated because as shown in the paper, increasing pitching moment results in an increase in $C_{l,\max}$. Also, the four design variables used in the paper are by no means the only choices. For example, the length of the transition ramps can be altered depending on the design Reynolds number or, say, the extent of lower-surface laminar flow can be altered independent of the upper surface.

Although the results of the parametric study are specific to the class of airplanes considered in the paper, the design approach and the design philosophies are applicable to a wide range of airplanes and other applications. In addition, the current work aims to satisfy a greater objective of showcasing the power of modern inverse design methods in tailoring an airfoil to suit a particular application.

Acknowledgment

The authors wish to thank Mark Drela for providing the XFOIL code used in this work.

References

[1]Holmes, B. J., Obara, C. J., and Yip, L. P., "Natural Laminar Flow Experiments on Modern Airplane Surfaces," NASA TP 2256, June 1984.

[2]Abbott, I. H., and von Doenhoff, A. E., *Theory of Wing Sections*, Dover, New York, 1959.

[3]Althaus, D., and Wortmann, F. X., *Stuttgarter Profilkatalog I*, Vieweg, Brunswick, Germany, 1981.

[4]Eppler, R., *Airfoil Design and Data*, Springer-Verlag, New York, 1990.

[5]Selig, M. S., and Maughmer, M. D., "A Multi-Point Inverse Airfoil Design Method Based on Conformal Mapping," *AIAA Journal*, Vol. 30, No. 5, 1992, pp. 1162–1170.

[6]Selig, M. S., and Maughmer, M. D., "Generalized Multipoint Inverse Airfoil Design," *AIAA Journal*, Vol. 30, No. 11, 1992, pp. 2618–2625.

[7]Drela, M., "XFOIL: An Analysis and Design System for Low Reynolds Number Airfoils," *Low Reynolds Number Aerodynamics*, edited by T. J. Mueller, Vol. 54 of *Lecture Notes in Engineering*, Springer-Verlag, New York, 1989, pp. 1–12.

[8]Drela, M., "Design and Optimization Method for Multi-Element Airfoils," AIAA Paper 93-0969, Feb. 1993.

[9]Wortmann, F. X., "Progress in the Design of Low Drag Airfoils," *Boundary Layer and Flow Control*, edited by G. V. Lachmann, Pergamon, London, 1961, pp. 748–770.

[10]Wortmann, F. X., "A Critical Review of the Physical Aspects of Airfoil Design at Low Mach Numbers," *Motorless Flight Research*, edited by J. L. Nash-Weber, NASA CR 2315, Nov. 1973.

[11]van Dam, C. P., and Holmes, B. J., "Boundary-Layer Transition Effects on Airplane Stability and Control," *Journal of Aircraft*, Vol. 25, No. 8, 1988, pp. 702–709.

[12]Somers, D. M., "Design and Experimental Results for a Natural-Laminar-Flow Airfoil for General Aviation Applications," NASA TP 1861, June 1981.

[13]Somers, D. M., "Design and Experimental Results for a Flapped Natural-Laminar-Flow Airfoil for General Aviation Applications," NASA TP 1865, June 1981.

[14]Somers, D. M., "Subsonic Natural-Laminar-Flow Airfoils," *Natural Laminar Flow and Laminar Flow Control*, edited by R. W. Barnwell and M. Y. Hussaini, Springer-Verlag, New York, 1992, pp. 143–176.

[15]Selig, M. S., Maughmer, M. D., and Somers, D. M., "A Natural-Laminar-Flow Airfoil for General-Aviation Applications," *Journal of Aircraft*, Vol. 32, No. 4, 1995, pp. 710–715.

[16]Giles, M. B., and Drela, M., "Viscous-Inviscid Analysis of Transonic and Low Reynolds Number Airfoils," *AIAA Journal*, Vol. 25, No. 10, 1987, pp. 1347–1355.